



UNIVERSITY OF LEEDS

This is a repository copy of *Adaptive high-order finite element solution of transient elastohydrodynamic lubrication problems*.

White Rose Research Online URL for this paper:
<http://eprints.whiterose.ac.uk/1786/>

Article:

Lu, H., Berzins, M., Goodyer, C. et al. (2 more authors) (2006) Adaptive high-order finite element solution of transient elastohydrodynamic lubrication problems. Proceedings of the Institution of Mechanical Engineers. Part J: Journal of engineering tribology, 220 (3). pp. 215-225. ISSN 1350-6501

<https://doi.org/10.1243/13506501JET134>

Reuse

See Attached

Takedown

If you consider content in White Rose Research Online to be in breach of UK law, please notify us by emailing eprints@whiterose.ac.uk including the URL of the record and the reason for the withdrawal request.



eprints@whiterose.ac.uk
<https://eprints.whiterose.ac.uk/>



White Rose
university consortium
Universities of Leeds, Sheffield & York

White Rose Consortium ePrints Repository

<http://eprints.whiterose.ac.uk/>

This is an author produced version of a paper published in **Proceedings of the Institution of Mechanical Engineers. Part J: Journal of engineering tribology.**

White Rose Repository URL for this paper:
<http://eprints.whiterose.ac.uk/1786/>

Published paper

Lu, H., Berzins, M., Goodyer, C., Jimack, P.K. and Walkley, M. (2006) *Adaptive high-order finite element solution of transient elastohydrodynamic lubrication problems*. Proceedings of the Institution of Mechanical Engineers. Part J: Journal of engineering tribology, 220 (3). pp.215-225.

Adaptive High-order Finite Element Solution of Transient Elastohydrodynamic Lubrication Problems

H Lu¹, M Berzins², CE Goodyer¹, PK Jimack^{1*} and M Walkley¹

¹ School of Computing, University of Leeds, UK

² Scientific Computing and Imaging Institute, University of Utah, USA

Abstract

This paper presents a new numerical method to solve transient line contact elastohydrodynamic lubrication (EHL) problems. A high-order Discontinuous Galerkin finite element method is used for the spatial discretization and the standard Crank-Nicolson method is employed to approximate the time derivative. An h-adaptivity method is used for grid adaptation with the time-stepping, and the penalty method is employed to handle the cavitation condition. The roughness model employed here is a simple indentation which is located on the upper surface. Numerical results are presented comparing the Discontinuous Galerkin method to standard finite difference techniques. It is shown that micro-EHL features are captured with far fewer degrees of freedom than when using low-order finite difference methods.

*Corresponding author: School of Computing, University of Leeds, UK

Keywords: high-order DG, adaptivity, EHL, line contact, transient.

Notation

b	Half-width Hertzian contact
G	dimensionless materials parameter
H	dimensionless film thickness
P	dimensionless pressure
p_h	maximum Hertzian pressure
p_0	ambient pressure
R	Reduced radius of curvature
\mathcal{R}	dimensionless deviations from the smooth profile
T	dimensionless time
u_s	sum velocity, $u_s = u_1 + u_2$
u_1	velocity of lower (smooth) surface
u_2	velocity of upper surface
\mathbf{u}	vector of finite element unknowns
U	dimensionless speed parameter
U_1	dimensionless velocity of lower (smooth) surface
U_2	dimensionless velocity of upper surface
W	dimensionless load parameter
X	dimensionless coordinate
X_d	dimensionless location of surface feature
X_s	dimensionless location of surface feature at $T = 0$
z	viscosity index
α	pressure viscosity index
ΔT	dimensionless time increment
η	dimensionless viscosity
η_0	viscosity at ambient pressure
λ	dimensionless speed parameter
ρ	dimensionless density

1 Introduction

Elastohydrodynamic Lubrication (EHL) problems have been studied for many years and many numerical methods have been introduced to solve them [1]-[8]. However, most of these methods are based around low order schemes and much of the algorithmic development behind them has focused on obtaining accuracy through the use of large numbers of discretization points by improving the efficiency and stability of the solvers used. In this work, improved accuracy is sought through the use of a higher order spatial representation of the solution. With this in mind, a relatively recent numerical method, Discontinuous Galerkin (DG) finite elements [9], was introduced by the authors in [10] to solve steady-state EHL problems. This method was shown to produce highly accurate numerical solutions with relatively few degrees of freedom. In this paper, the high order DG method is generalised to solve transient line contact problems, combined with the Crank-Nicolson time discretization [11]. The resulting numerical simulations capture far greater detail in the pressure profile than has been previously observed with such a small number of degrees of freedom.

This paper is organised as follows. In this section, a brief introduction to numerical methods for EHL problems is given. Section 2 begins from the governing equations for a non-dimensionalized 1D transient EHL problem. A description of the high order DG spatial discretization and Crank-Nicolson time-stepping follows. In order to reduce the computational expense, a spatial adaptivity method is also introduced in this section. Numerical results are given in Section 3. Finally, the main conclusions of the paper are summarised in Section 4.

1.1 EHL Problems

In order to reduce the power loss caused by friction, a lubricant is used to separate the contacting elements in most modern machines. An important effect that often occurs during this separation is elastohydrodynamic lubrication. EHL problems are

characterised by the significant elastic deformation of the contacting surfaces and the dramatic increase in the viscosity of the lubricant with increasing pressure [12].

After several significant breakthroughs [1]-[8], EHL contact problems for perfectly smooth surfaces are now relatively well understood. In 1951, Petrusevich [12] obtained the first numerical solution of the steady-state line contact problem containing all of the main features of EHL solutions. In his results, the second maximum in the pressure profile was first obtained, which now is referred to as “the Petrusevich spike” or “the pressure spike”, and a corresponding dip in film thickness was also observed. With more robust numerical methods [1]-[8], more accurate numerical solutions of steady-state EHL contact problems have been presented. Consequently, precise solutions for a wide range of loaded cases can be obtained using numerical methods.

However, in practice, the contacting surfaces will not be perfectly smooth. As a result, the roughness on the surfaces should be taken into account. Furthermore, a transient analysis is required since the roughness in the contact will vary due to the moving surfaces. This is generally referred to as a micro-EHL contact problem [11, 13]. For theoretical analysis, artificial roughness models (such as indentation or waviness) [13] are usually adopted. In some situations, real roughness can also be handled using numerical methods [11]. Numerical results show that the roughness can strongly affect the pressure distribution and the film thickness profile and that the transient solutions might therefore be significantly different from their steady state counterparts. It follows that transient analysis is of great importance in order to be able to approach reliable numerical predictions of the real behaviour of the lubricant.

1.2 Numerical Methods for EHL

A significant breakthrough that has possibly done more than any other to improve the efficiency and robustness of EHL solvers in recent years is the application of the multi-grid method. This is able to accelerate the convergence of solution algorithms signif-

icantly because it is effective at eliminating both high-frequency and low-frequency error components by using a sequence of grids. Multigrid was first applied to EHL problems by Lubrecht *et al.* in 1986 [6], combined with Gauss-Seidel relaxation. Furthermore, a multilevel multi-integration algorithm was developed for the fast calculation of the film thickness [1, 7]. Venner [7, 8] and Nurgat [14] each introduced new relaxation methods which makes the multigrid method more robust. Both methods can handle a large range of loaded cases and make it possible to obtain accurate numerical solutions by using many grid points. Since the multilevel techniques can significantly accelerate the computation, it is also possible to obtain transient solutions in a relatively short time [13].

Prior to the wide spread use of multilevel solvers a popular approach for the stable solution of highly loaded problems was the inverse method [2]-[4]. The Reynolds equation is used to calculate the film thickness from a given pressure profile, which is then updated based on the difference between this thickness and that calculated from the film thickness equation. It turns out however that the inverse method is only suitable for highly loaded cases and is not sufficiently robust to solve a wide range of EHL problems. Furthermore, the application of the inverse method to rough contact problems is challenging since the inverse pressure is calculated based on the difference between the hydrodynamic film thickness and the elastic film thickness which is not sensitive to any local change in pressure. Another well-known method is the Newton-Raphson approach in which the Reynolds equation is linearised and the resulting Jacobian matrix, which consists of the derivatives of all discrete equations with respect to all variables, is used to update the solution. One significant advantage is that a converged solution is obtained quickly. However a good initial guess is required and the implementation of the cavitation condition is rather complex. Based on this, a coupled method [15, 16] was introduced to improve the relaxation robustness. Instead of calculating the film thickness and the pressure in separate stages, the discrete Reynolds

equation and the discrete film thickness equation are coupled into one discrete system and both the pressure and the film thickness are treated as active variables and updated simultaneously. In order to simplify the resulting discrete system, the differential deflection method [17] was introduced to relate the pressure and the deflection in an alternative differential form.

For all of the above mentioned relaxation methods, the most widely used spatial discretization is the finite difference (FD) method. As an alternative, the continuous spatial finite element method has also been successfully applied to solve incompressible EHL problems [18]-[24]. However, experiences of applying traditional continuous finite element methods to the compressible Reynolds equation, especially with higher than first order elements [16], have tended to yield unphysical oscillatory pressure profiles in the contact region. In the following section a discontinuous finite element discretization is introduced in order to overcome this difficulty.

2 High Order DG for EHL

The key features of an EHL solution can be captured using the numerical methods previously discussed, such as: the low pressure inlet region; a rapid rise in pressure through the centre of the contact, typically reaching the giga-Pascal range; a cavitation boundary in the outflow; and, a sharp pressure spike past the centre of the contact, towards the outflow. It has been shown that if this spike is not resolved sufficiently accurately then the calculated friction can be inaccurate [25]. However, all of the widely used numerical algorithms are low order schemes. Consequently the only available option to improve accuracy is to increase the number of grid points, which increases the computational expense. As an alternative to these low order methods, a high order DG method has been introduced to solve steady-state EHL line contact problems in [10]. Numerical experiments show that this method is stable across a wide range of loads and permits accurate solutions using a relatively small number of degrees of freedom,

provided suitable grids are used.

In this paper, this high order DG method is extended to the solution of transient line contact problems. An automatic h-adaptivity method is introduced to improve the accuracy, and a penalty method, first introduced by Wu [24], is employed to handle the cavitation boundary. The accuracy of this high order DG method allows very detailed features of the transient line contact problem considered to be captured and these are reported in Section 3.

2.1 Governing Equations

In [7] a dimensionless mathematical model of an isothermal EHL line contact problem is presented. This consists of three equations: the Reynolds equation, the film thickness equation and the force balance equation. The Reynolds equation reads:

$$\frac{\partial}{\partial X} \left(\epsilon \frac{\partial P}{\partial X} \right) - \frac{\partial(\rho H)}{\partial X} - \frac{\partial(\rho H)}{\partial T} = 0, \quad (1)$$

where $\epsilon = \frac{\rho H^3}{\eta \lambda}$, $P(X)$ and $H(X)$ are the unknown pressure and film thickness, $\rho(P)$ and $\eta(P)$ are the density and viscosity, and λ is a dimensionless speed parameter.

The elasticity and the roughness are included through the film thickness equation which defines the contact geometry for a given pressure solution:

$$H(X, T) = H_{00}(T) + \frac{X^2}{2} - \mathcal{R}(X, T) - \frac{1}{\pi} \int_{-\infty}^{\infty} \ln |X - X'| P(X', T) dX', \quad (2)$$

where H_{00} is the central offset film thickness and the integral describes the elastic deformation. $\mathcal{R}(X, T)$ describes the surface roughness. In this work the same dimensionless model of the roughness is adopted as was used by Venner in [13]:

$$\mathcal{R}(X, T) = \alpha 10^{-10((X-X_d))^2} \cos(2\pi(X - X_d)), \quad (3)$$

where $\alpha = -0.11$ is the amplitude. At time T , the position of the centre of the dent X_d is given by:

$$X_d = X_s + 2\frac{u_2}{u_s}T, \quad (4)$$

where X_s denotes the position of the dent at $T = 0$ and u_2 and u_s are the velocity of the upper surface, which is indented, and the sum velocity respectively. For all of the calculations described in this paper $\frac{u_2}{u_s} = 0.25$, hence some sliding behaviour is implied.

The force balance equation is a conservation law for the applied load, given by:

$$\int_{-\infty}^{\infty} P(X) dX - \frac{\pi}{2} = 0. \quad (5)$$

The lubricant rheology is also highly non-linear in pressure. In this work the viscosity-pressure relationship of Roelands [7] has been used:

$$\eta(P) = e^{\left\{\frac{\alpha p_0}{z}[-1+(1+\frac{Pp_h}{p_0})^z]\right\}}, \quad (6)$$

where $z = 0.6$ is the viscosity index, $\alpha = 2.165 \times 10^{-8}$ is the pressure viscosity index, and $p_0 = 1.98 \times 10^8$ is ambient pressure. The density model of Dowson and Higginson(see [7]) is used to describe the compressibility of the lubricant:

$$\rho(P) = \frac{0.59 \times 10^9 + 1.34Pp_h}{0.59 \times 10^9 + Pp_h}, \quad (7)$$

where p_h is the maximum Hertzian pressure.

For physical reasons, all pressures should be larger than or equal to the vapour pressure of the lubricant (zero). However, the Reynolds equation allows the pressure in the outlet region to decrease without limit if the outlet boundary X_{outlet} is far enough from the contact region. Consequently, the outlet boundary is therefore treated as a free

boundary. The boundary conditions are:

$$P(X_{inlet}) = 0, \quad P(X_{outlet}) = 0 \quad \text{and} \quad \frac{dP}{dX}(X_{outlet}) = 0, \quad (8)$$

where X_{inlet} denotes the inlet boundary position, located far enough from the contact region to approximate an infinite upstream boundary.

2.2 Spatial Discretization

Let Ω_h be a partition of the domain $\Omega = [X_{inlet}, X_{outlet}]$ into N elements. Let $\Gamma_{int} = \cup \Gamma_{ef}$ denote internal interfaces between elements, where Γ_{ef} is the grid point separating elements e and f . The jump of a function v on the element interface Γ_{ef} is defined as:

$$[v]_{ef}(x) = \lim_{x \rightarrow \Gamma_{ef}, x \in e} v - \lim_{x \rightarrow \Gamma_{ef}, x \in f} v, \quad e > f, \quad (9)$$

and the average

$$\langle v(x) \rangle_{ef} = \frac{1}{2} \left(\lim_{x \rightarrow \Gamma_{ef}, x \in e} v + \lim_{x \rightarrow \Gamma_{ef}, x \in f} v \right). \quad (10)$$

In each element e , P is approximated in the following form:

$$P^e(X) = \sum_{i=1}^{p^e+1} u_i^e N_i^e(X), \quad N_i^e(X) \in V \quad (11)$$

where p^e is the order of the approximating polynomial, u_i^e are the unknown coefficients and $N_i^e(X)$ are the local finite element basis functions which belong to a finite element space V . As discussed in [10], the steady-state 1D Reynolds equation can be discretized into the following form using Oden's DG scheme [9]:

$$L(P, v) = a(P, v) - l(P, v) = 0, \quad \forall v \in V, \quad (12)$$

where

$$\begin{aligned}
a(P, v) = & \sum_{e \in \Omega_h} \left(\int_e \epsilon \frac{\partial P}{\partial X} \frac{\partial v}{\partial X} dX \right) + \sum_{\Gamma_{int}} \left([v] \left\langle \left(\epsilon \frac{\partial P}{\partial X} \right) \right\rangle - [P] \left\langle \left(\epsilon \frac{\partial v}{\partial X} \right) \right\rangle \right) \\
& + \left(v \epsilon \frac{\partial P}{\partial X} \right) \Big|_{X_{inlet}} - \left(v \epsilon \frac{\partial P}{\partial X} \right) \Big|_{X_{outlet}} - \left(P \epsilon \frac{\partial v}{\partial X} \right) \Big|_{X_{inlet}} + \left(P \epsilon \frac{\partial v}{\partial X} \right) \Big|_{X_{outlet}}, \tag{13}
\end{aligned}$$

and

$$\begin{aligned}
l(P, v) = & \sum_{e \in \Omega_h} \left(\int_e \rho H \frac{\partial v}{\partial X} dx \right) + \sum_{\Gamma_{int}} [v] \langle \rho(P^-) H \rangle \\
& + (\rho H v) \Big|_{X_{inlet}} - (\rho H v) \Big|_{X_{outlet}} - \left(g_{inlet} \epsilon \frac{\partial v}{\partial X} \right) \Big|_{X_{inlet}} + \left(g_{outlet} \epsilon \frac{\partial v}{\partial X} \right) \Big|_{X_{outlet}}. \tag{14}
\end{aligned}$$

In the above equations,

$$P^- = \lim_{\sigma \rightarrow 0} P(x - \sigma), \text{ for } x \in \Gamma_{int}. \tag{15}$$

This provides sufficient upwinding to ensure a stable solution [9].

As discussed in [10], for a given pressure distribution the film thickness may be calculated as follows:

$$H(X, T) = H_{00}(T) + \frac{X^2}{2} - \mathcal{R}(X, T) - \frac{1}{\pi} \sum_{e=1}^N \sum_{i=1}^{p^e+1} K_i^e(X) u_i^e(T), \tag{16}$$

where the $K_i^e(X)$ are defined by:

$$K_i^e(X) = \int_e \ln |X - X'| |N_i^e(X')| dX'. \tag{17}$$

Here $K_i^e(X)$ is estimated using numerical integration: for $X \in e$ singular quadrature [26] is employed since $\ln |X - X'|$ has a weak singularity at $X' = X$; elsewhere

Gaussian quadrature is satisfactory.

The force balance equation is discretized according to:

$$\sum_{e=1}^N \int_e \sum_{i=1}^{p^e+1} u_i^e(T) N_i^e(X) dX - \frac{\pi}{2} = 0. \quad (18)$$

2.3 Penalty Method

A grid-moving method has been used by the authors to capture the cavitation position in [10] for line contact problems, which can give a very accurate cavitation position. However, it slows down the convergence since it is necessary to keep moving the grid to find the cavitation position, and the accuracy of the initial guess of the cavitation position can strongly affect the convergence speed. In this work, the Penalty method [24] is employed to handle the cavitation condition, which significantly simplifies the treatment of the free boundary, which is of course transient for time dependent problems.

The Penalty method was introduced by Wu [24] in 1986 and was successfully applied to the nonlinear EHL Reynolds-Hertz problem to handle the free boundary. Instead of finding the exact cavitation position [10], the penalty method treats the cavitation condition weakly, which simplifies the numerical scheme. By introducing an exterior penalty term, the following nonlinear system should now be solved instead of (12):

$$L(P, v) = a(P, v) + \frac{1}{\delta} \langle P^-, v \rangle - l(P, v) = 0, \quad (19)$$

where δ is an arbitrary positive number ($\delta = 1.0 \times 10^{-7}$ here),

$$P^- = \min(P, 0) \quad \text{and} \quad \langle P^-, v \rangle = \sum_{e \in \Omega_h} \left(\int_e P^- v dx \right). \quad (20)$$

Note that the penalty term $\frac{1}{\delta} \langle P^-, v \rangle$ has no effect where $P \geq 0$. However, in the outlet region, where $P < 0$, the penalty term dominates equation (19), provided that δ is sufficiently small. In this case, the negative pressures are forced to be zero by

the presence of the penalty term in this modified weak form. From an implementation point of view, the only modification required is to take account of the penalty term when discretizing the Reynolds equation. The physical constraint that $P \geq 0$ over the entire computational domain is then satisfied automatically and the cavitation position is located at the least value of X for which $P(X) = 0$.

Using (11), the steady-state equation (19) can be written in the general nonlinear form [10]:

$$\mathbf{L}(\mathbf{u}) = \mathbf{A}(\mathbf{u})\mathbf{u} - \mathbf{b}(\mathbf{u}) = \mathbf{0}, \quad (21)$$

where

$$\mathbf{u} = (u_1^1, \dots, u_{p^1+1}^1; \dots; u_1^N, \dots, u_{p^N+1}^N). \quad (22)$$

2.4 Temporal Discretization

Using the Crank-Nicolson method [11] and the DG spatial discretization (19), the 1D transient Reynolds equation is discretized to be:

$$\begin{aligned} - \sum_{e \in \Omega_h} \left(\int_e \rho H v dx \right)^T + \sum_{e \in \Omega_h} \left(\int_e \rho H v dx \right)^{T+\Delta T} \\ + \theta \Delta T L(P, v)^T + (1 - \theta) \Delta T L(P, v)^{T+\Delta T} = 0, \quad \forall v \in V, \quad (23) \end{aligned}$$

where $\theta = 0.5$ here. Reorganising the above equations, yields the following discrete form:

$$\begin{aligned} \sum_{e \in \Omega_h} \left(\int_e \rho H v dx \right)^{T+\Delta T} + (1 - \theta) \Delta T L(P, v)^{T+\Delta T} = \\ \sum_{e \in \Omega_h} \left(\int_e \rho H v dx \right)^T - \theta \Delta T L(P, v)^T. \quad (24) \end{aligned}$$

To simplify the notation, using (11), the above system is rewritten as:

$$\mathbf{R}^{T+\Delta T} = \mathbf{C}(\mathbf{u}^{T+\Delta T}) + (1-\theta)\Delta T \mathbf{L}(\mathbf{u}^{T+\Delta T}) - \mathbf{C}(\mathbf{u}^T) + \theta\Delta T \mathbf{L}(\mathbf{u}^T) = \mathbf{0}, \quad (25)$$

where \mathbf{L} is given by (21), $\mathbf{C}(\mathbf{u}^{T+\Delta T})$ has components $(\int_e \rho H N_i^e dx)^{T+\Delta T}$, $\mathbf{C}(\mathbf{u}^T)$ has components $(\int_e \rho H N_i^e dx)^T$, and

$$\mathbf{u}^{T+\Delta T} = ((u_1^1)^{T+\Delta T}, \dots, (u_{p^1+1}^1)^{T+\Delta T}; \dots; (u_1^N)^{T+\Delta T}, \dots, (u_{p^N+1}^N)^{T+\Delta T}) \quad (26)$$

are the unknown pressure coefficients. Similar to the nonlinear smoother introduced in [10], the following relaxation method is used for the iterative solver at each time step in this paper:

$$\mathbf{u}^{T+\Delta T} \leftarrow \mathbf{u}^{T+\Delta T} + \left(\frac{\partial (\mathbf{C}(\mathbf{u}^{T+\Delta T}) + (1-\theta)\Delta T \mathbf{L}(\mathbf{u}^{T+\Delta T}))}{\partial \mathbf{u}^{T+\Delta T}} \right)^{-1} \mathbf{R}^{T+\Delta T}, \quad (27)$$

where $\mathbf{R}^{T+\Delta T}$ is the numerical residual and the Jacobian, $\frac{\partial \mathbf{L}(\mathbf{u}^{T+\Delta T})}{\partial \mathbf{u}^{T+\Delta T}}$, is approximated by:

$$\frac{\partial \mathbf{L}(\mathbf{u}^{T+\Delta T})}{\partial \mathbf{u}^{T+\Delta T}} \approx \mathbf{A}(\mathbf{u}^{T+\Delta T}) - \frac{\partial \mathbf{b}(\mathbf{u}^{T+\Delta T})}{\partial \mathbf{u}^{T+\Delta T}}. \quad (28)$$

Both $\frac{\partial \mathbf{C}(\mathbf{u}^{T+\Delta T})}{\partial \mathbf{u}^{T+\Delta T}}$ and $\frac{\partial \mathbf{b}(\mathbf{u}^{T+\Delta T})}{\partial \mathbf{u}^{T+\Delta T}}$ are full since the film thickness at any position depends on all pressures.

2.5 Adaptivity

The finite element functions, N_i^e , used in this work are the hierarchical basis functions described in [27]. Specifically, in the reference element ($-1 \leq \xi \leq 1$) the basis functions are defined as follows:

$$N_1(\xi) = \frac{1-\xi}{2}; N_2(\xi) = \frac{1+\xi}{2}; N_i(\xi) = \phi_{i-1}(\xi), \quad i = 3, 4, \dots, p+1 \quad (29)$$

where p is the polynomial degree of the elements and ϕ_j is defined in terms of the Legendre polynomial P_{j-1} :

$$\phi_j(\xi) = \sqrt{\frac{2j-1}{2}} \int_{-1}^{\xi} P_{j-1}(t) dt, \quad j = 2, 3, \dots \quad (30)$$

The basis functions N_1 and N_2 are called nodal shape functions or external modes. The basis functions $N_i, i = 3, 4, \dots, p+1$ are called internal shape functions or internal bubble modes. The bubble modes can be viewed as corrections to the nodal shape functions, which can improve the accuracy of the solution on the current element. Numerical experiments suggest that the high order coefficients u_i^e , corresponding to the higher order basis functions, are usually very small when an accurate, converged solution is obtained. When the local order of the basis functions is not high enough, or the local mesh is not fine enough, these high order coefficients are relatively large and the resulting solution is not sufficiently accurate. Based on this property of the basis functions, an h-adaptivity method has been implemented, through which the grid is adjusted during the computation to ensure the accuracy of the solution at every time step. Note that in this work the same order is used over the entire domain, however more generality is easily possible.

The basic principle behind the adaptivity is summarised as follows:

1. Refine any element on which the solution has too large a contribution from the highest order basis functions. A small tolerance Tol_{refine} is chosen such that if either of the last two high order coefficients ($u_{p^e}^e$ and $u_{p^e+1}^e$) is greater than Tol_{refine} , then the element e is divided into two equally sized smaller elements.
2. Agglomerate two neighbouring elements to be a larger one if the local solution is sufficiently smooth. Here, each pair of neighbouring elements (for example e and $e+1$), are agglomerated into a larger trial element E , and the local solution is interpolated onto the trial element. If the both of the coefficients $u_{p^E}^E$ and $u_{p^E+1}^E$

are less than another tolerance $Tol_{coarsen} < Tol_{refine}$, take E as the new local mesh element to replace e and $e + 1$.

Figure 1 shows a schematic of the refinement and coarsening operations. Note that in principle it is possible to constrain the mesh adaptivity to ensure that no two neighbouring elements differ in size by more than a predetermined ratio. This has not been found to be necessary for the one-dimensional examples reported in this work however it is a relatively straightforward constraint to impose. When undertaking refinement it is necessary to check the size of neighbouring elements and also mark them for refinement if they are too large. Similarly, when coarsening a mesh it is necessary to begin with the smallest elements and check that their neighbours are not too small to prevent the constraint from being violated: if the neighbours are too small then the coarsening is not undertaken.

2.6 Overall Solution Procedure

A sequence of numerical solutions at different time steps are calculated as follows.

1. At the start, the dent is located far from the contact region. The steady state solution at $T = 0$ is used as the initial solution. Then for each time step, repeat 2–5 below.
2. Choose $\mathbf{u}^{T+\Delta T} = \mathbf{u}^T$ as initial guess.
3. Update $\mathbf{u}^{T+\Delta T}$ by using (27) repeatedly until convergence to an intermediate tolerance.
4. Check if the grid needs to be adapted. If yes, go to step 3 after generating the new grid according to the h-adaptivity method discussed above and transferring both $\mathbf{u}^{T+\Delta T}$ and \mathbf{u}^T onto the new grid.
5. Update $\mathbf{u}^{T+\Delta T}$ by using (27) repeatedly until convergence to a final tolerance.

Note that it is necessary to check the degree of smoothness for both $u^{T+\Delta T}$ and u^T on the local trial element when determining whether to coarsen the local mesh. The local mesh is coarsened only if both of the local solutions at T and $T + \Delta T$ are sufficiently smooth.

3 Numerical Results

Note that a comparison of the DG method against standard finite difference results, with very fine computational grids, is presented for steady-state problems in [10]. Hence such a comparison is not repeated here. Instead, the focus is on the solution of a challenging transient model problem using the DG scheme and demonstrate that it is capable of resolving details of the solution that are not so easily captured by a more traditional finite difference scheme with a similar number of degrees of freedom.

In this section, the new numerical scheme for compressible EHL is therefore used to investigate the influence of a dent on the upper surface on the pressure and the film thickness under certain conditions. In standard Dowson and Higginson notation the case solved here is specified by the non-dimensional quantities, $U = 0.15^{-11}$, $W = 0.4 \times 10^{-4}$, $G = 4942$ (see [7]). The computational domain is $[-5.0, 1.5]$. The roughness model used is given by (3).

When $T = 0$, where $X_d = -2.0$ (relatively far from the contact centre), the pressure and film thickness, depicted on the left in Figure 2, are quite similar to the steady-state solution of the smooth contact. A detailed view of the pressure spike captured by DG and FD is shown on the right in Figure 2. Note that the FD solutions for which the grid points are equally spaced converge toward the DG solution ($p^e = 8$ everywhere, 37 elements and 333 unknowns in total) with increasing number of grid points. Indeed, it is seen that the DG method resolves the pressure spike more accurately than FD, as in [10]. Furthermore, when the DG method is applied with even higher degree approximating polynomials (e.g. $p^e = 10$) the steady-state initial solution that is obtained is

virtually identical to that shown in Figure 2, suggesting that $p^e = 8$ provides sufficient accuracy for this problem.

Figure 3 shows a sequence of solutions with the dent moving. Note that in Figure 3(b) a new pressure spike is captured (at approximately $X = -0.9$), which is caused by the roughness. This becomes sharper and then begins to disappear in Figure 3(c). After the dent passes the contact centre, this spike grows up again (see Figure 3(d) and 3(e)). When the dent centre arrives at the “Petrusevich Spike” region, the combination of the roughness and the film thickness dip produces a much sharper pressure spike (see Figure 3(f)).

At each time step, the number of the elements remains no more than 60 since h-adaptivity is employed. Since $p^e = 8$ everywhere the total number of degrees of freedom never exceeds 540. It should be noted however that the time step has to be quite small ($\Delta T = 0.001$ when the pressure profile is relatively smooth and $\Delta T = 0.0001$ when the sharp spike appears and small elements are required to resolve it). Other DG simulations have been carried out using different time steps and different order basis functions and in each case, provided that p^e is sufficiently large and the time step is sufficiently small, the qualitative features of the solution are unchanged. In particular, the pressure spike that is caused by the roughness is evident in all of these simulations and does not appear to be a numerical artifact.

In order to further illustrate the potential of this method, results are also included when computed using the standard multilevel finite difference scheme [5, 7] on a moderately sized grid of 1025 points. Figure 4 shows the history of the pressure spike caused by the roughness, which has not been captured by the multilevel FD method. Note that there is no spike in Figure 4 (a) when $X_d = -0.9$, but the roughness has significantly affected the pressure profile. From Figure 4(b) to (f), the spike has been clearly captured by the DG method and completely missed by the FD method. It should be noted that elsewhere in the domain there is good agreement between the two solu-

tions.

It is important to note that the implications of this additional accuracy in the DG scheme are that useful quantities, such as friction [25], can be computed with greater accuracy at relatively low resolution. The friction is given by:

$$F = \int_{X_{inlet}}^{X_{outlet}} -m_1 \frac{dP}{dX} \frac{H}{2} + m_2 \frac{\eta}{H} (U_2 - U_1) dX, \quad (31)$$

where $m_1 = \frac{p_h b^2}{R}$ and $m_2 = \frac{\eta_0 R}{b}$. Table 1 shows a comparison of this non-dimensional friction calculated from the DG solutions and the FD solutions. At times in the simulation where the micro-EHL spike is apparent, the solution computed by the FD scheme, which misses the spike, is up to 20% different from the DG solution. This is due to both the significant discrepancy in $\frac{dP}{dX}$ in the rolling term and the large difference in η (which depends exponentially on P , see Equation (6)) in the sliding term of the friction equation (31).

4 Conclusions

A high order DG method introduced by the authors for the solution of steady-state problems in [10] has been extended to solve transient line contact EHL problems. Here, the efficiency of the implementation of the DG solver has not been considered, through the potential use of multilevel multi-integration for example, [1, 7]. The work presented in this paper should therefore be viewed as provisional results which are indicative of the potential of the DG method for transient EHL problems rather than a well-tuned algorithm and implementation.

Through the high accuracy of the DG method and its flexibility in adaptivity, it is shown that additional details of the solution may be captured, compared to the traditional finite difference method. Particularly, due to the roughness profile, a micro-EHL pressure spike has been captured in addition to the well-known ‘‘Petrusevich Spike’’

using less than 540 degrees of freedom.

The employment of the penalty method makes it simple to handle the cavitation condition. Note that the DG approach may also be applied in conjunction with other numerical schemes for treating the free boundary, e.g. [10], or possibly even with fundamentally different numerical approaches, such as the coupled method [15, 16]. One particular advantage of the penalty method, used to treat the free boundary here, is that it extends naturally to point contact problems in two dimensions. Currently work is in progress on the solution of point contact problems, using p-multigrid [28] to accelerate the convergence. In this case, the calculation of the elastic deformation is far more expensive than in 1D, hence some form of fast multilevel multi-integration must be implemented. The use of adaptive time-stepping [29] will also be essential for transient point contact problems.

References

- [1] **Brandt, A. and Lubrecht, A.A.** Multilevel matrix multiplication and fast solution of integral equations. *J. Comput. Phys*, 1990, **90**, 348-370.
- [2] **Dowson, D. and Higginson, G.R.** A numerical solution to the elastohydrodynamic problem. *Journal of Mechanical Engineering Science*, 1959, **1**(1), 6-15.
- [3] **Evans, H.P. and Snidle, R.W.** Inverse solution of Reynolds' equation of lubrication under point-contact elastohydrodynamic conditions. *Trans. ASME, Journal of Tribology*, 1981, **103**, 539-546.
- [4] **Evans, H.P. and Snidle, R.W.** The elastohydrodynamic lubrication of point contact at heavy loads. *Proc. R. Soc. Lond. A*, 1982, **382**, 183-199.
- [5] **Goodyer, C.E.** Adaptive numerical methods for elastohydrodynamic lubrication. PhD thesis, University of Leeds, Leeds UK, 2001.

- [6] **Lubrecht, A.A., Ten Napel, W.E. and Bosma, R.** Multigrid, an alternative method for calculating film thickness and pressure profiles in elasto-hydrodynamically lubricated line contacts. *Trans. ASME, Journal of Tribology*, 1986, **108**, 551-556.
- [7] **Venner, C.H.** Multilevel solution of the EHL line and point contact problems. PhD thesis, University of Twente, Enschede, The Netherlands, 1991.
- [8] **Venner, C.H.** Higher-order multilevel solvers for the EHL line and point contact problem. *Trans. ASME, Journal of Tribology*, 1994, **116**, 741-750.
- [9] **Baumann, C.E. and Oden, J.T.** A discontinuous hp finite element method for convection-diffusion problems. *Comput. Methods. Appl. Mech. Engrg.*, 1999, **175**, 311-341.
- [10] **Lu, H., Berzins, M., Goodyer, C.E. and Jimack, P.K.** High order discontinuous Galerkin method for EHL line contact problems. *Communications in Numerical Methods in Engineering*, 2005, **21**, 643-650.
- [11] **Elcoate, C.D., Evans, H.P., Hughes, T.G. and Snidle, R.W.** Transient elasto-hydrodynamic analysis of rough surfaces using a novel coupled differential deflection method. *Proc. Instn. Mech. Engrs*, 2001, **215**, 319-337.
- [12] **Petrusevich, A.I.** Fundamental conclusions from the contact-hydrodynamic theory of lubrication. *Izv. Akad. Nauk. SSSR (OTN)*, 1951, **2**(209).
- [13] **Venner, C.H. and Lubrecht, A.A.** Transient analysis of surface features in an EHL line contact in the case of sliding. *Journal of Tribology*, 1994, **116**, 186-193.
- [14] **Nurgat, E., Berzins, M. and Scales, L.E.** Solving EHL problems using iterative, multigrid and homotopy Methods. *Journal of Tribology*, 1999, **121**, 28-34.

- [15] **Elcoate, C.D., Evans, H.P. and Hughes, T.G.** On the coupling of the elastohydrodynamic problem. *Proc. Instn Mech. Engrs. Part J. Journal of Engineering Tribology*, 1998, **212**, 307-318.
- [16] **Hughes, C.D., Elcoate, T.G. and Evans, H.P.** A novel method for integrating first and second order differential equations in elastohydrodynamic lubrication for the solution of smooth isothermal, line contact problems. *International Journal for Numerical Methods in Engineering*, 1999, **44**, 1099-1113.
- [17] **Evans, H.P. and Hughes, T.G.** Evaluation of deflection in semi-infinite bodies by a differential method. *Proc. Instn Mech. Engrs. Part J. Journal of Engineering Tribology*, 2000, **214**, 563-584.
- [18] **Rohde, S.M. and Oh, K.P.** A unified treatment of thick and thin film elastohydrodynamic problems by using higher order element methods. *Proc. R. Soc. Lond. A.*, 1975, **343**, 315-331.
- [19] **Taylor, C. and O'Callaghan, J.F.** A numerical solution of the elastohydrodynamic lubrication problem using finite elements. *Journal of Mechanical Science*, 1972, **14**, 229-237.
- [20] **Hamrock, B.J., Hsiao, HS.S. and Tripp, J.H.** Finite element system approach to EHL of elliptical contacts: Part 1 - isothermal circular non-Newtonian formulation. *Trans. ASME, Journal of Tribology*, Oct 1998, **120**, 695-704.
- [21] **Hamrock, B.J., Hsiao, HS.S. and Tripp, J.H.** Finite element system approach to EHL of elliptical contacts: Part 2 - isothermal results and performance formulas. *Trans. ASME, Journal of Tribology*, Oct 1999, **121**, 711-720.
- [22] **Nguyen, S.H.** A higher-order finite element scheme for incompressible lubrication calculations. *Finite Elements in Analysis and Design*, 1992, **10**, 307-317.

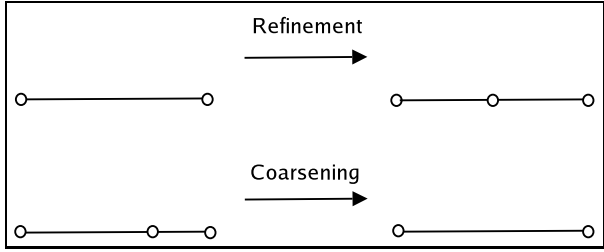
- [23] **Oh, K.P. and Rohde, S.M.** Numerical solution of the point contact problem using the finite element method. *International Journal for Numerical Methods in Engineering*, 1977, **11**, 1507-1518.
- [24] **Wu, S.R.** A penalty formulation and numerical approximation of the Reynolds-Hertz problem of elastohydrodynamic lubrication. *Int. J. Eng. Sci.*, 1986, **24**(6), 1001-1013.
- [25] **Goodyer, C.E., Fairlie, R., Hart, D.E., Berzins, M. and Scales, L.E.** Calculation of friction in steady-state and transient EHL simulations In A. Lubrecht *et al.*, editor, *Transient Processes in Tribology: Proceedings of the 30th Leeds-Lyon Symposium on Tribology*. Elsevier, 2004, 579–590.
- [26] **Evans, G.** Practical numerical integration. John Wiley Sons, Chichester, England, 1993.
- [27] **Szabo, B. and Babuska, I.** Finite element analysis. Wiley, New York, 1991.
- [28] **Fidkowski, K.J. and Darmofal, D.L.** Development of a higher-order solver for aerodynamic applications. *42nd AIAA Aerospace Sciences Meeting and Exhibit, AIAA Paper*, 2004, 2004-0436.
- [29] **Goodyer, C.E. and Berzins, M.** Adaptive timestepping for elastohydrodynamic lubrication solvers *SIAM Journal on Scientific Computing*, in press.

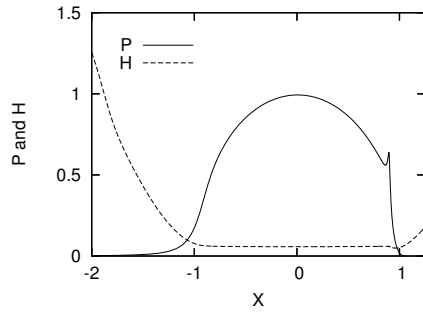
List of Figures

1	H-adaptivity	24
2	Non-dimensional pressure and film thickness when $X_d = -2.0$	25
3	Non-dimensional pressure and film thickness obtained using the DG method	26
4	Comparison of the fine details of the pressure computed via the new Discontinuous Galerkin method and using the standard multilevel finite difference solver on a mesh of 1025 points	27

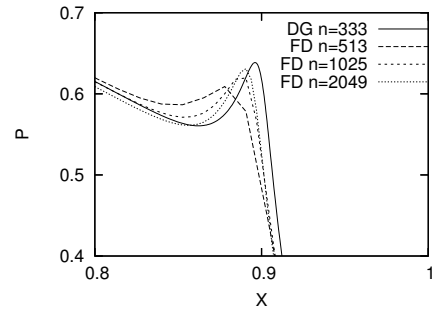
List of Tables

1	Comparison of non-dimensional friction at particular times	28
---	--	----

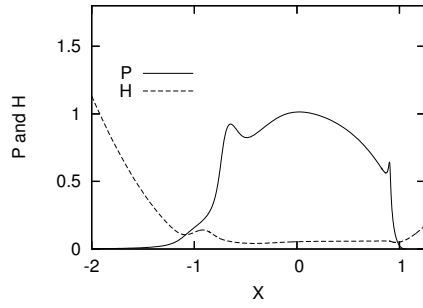




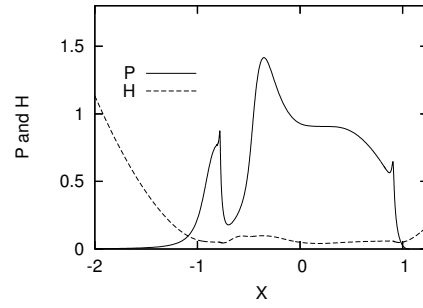
(a) DG solution



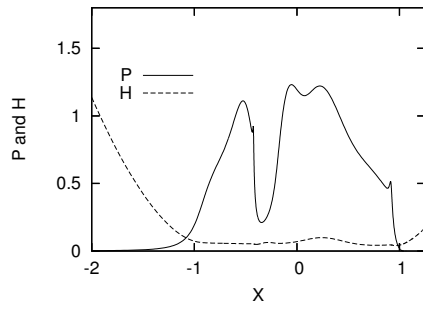
(b) Resolution of the pressure spike using DG (333 degrees of freedom) and FD (513 to 2049 degrees of freedom)



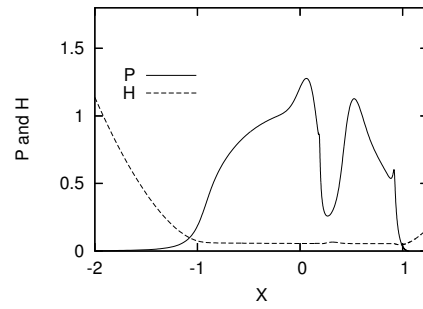
(a) $X_d = -0.9$



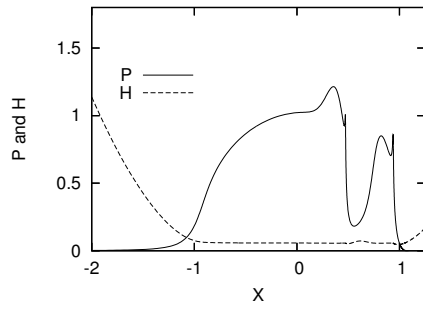
(b) $X_d = -0.6$



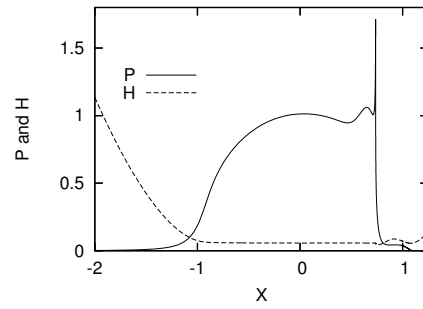
(c) $X_d = -0.3$



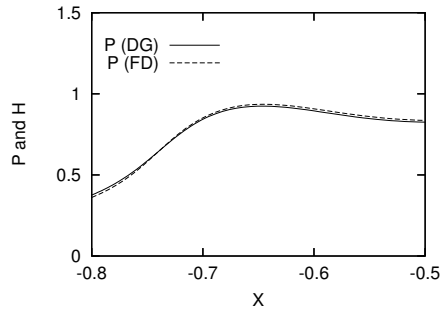
(d) $X_d = 0.3$



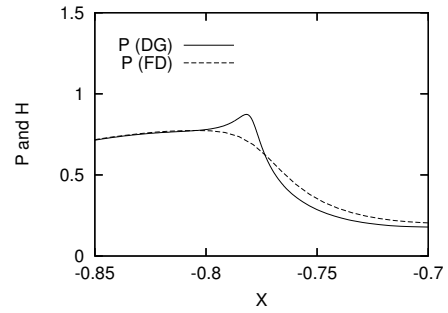
(e) $X_d = 0.6$



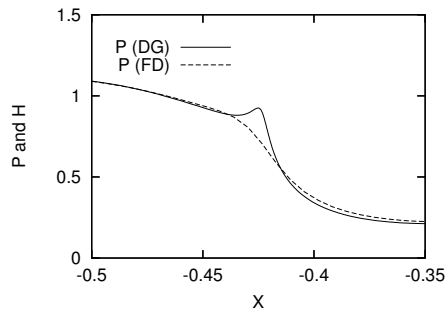
(f) $X_d = 0.9$



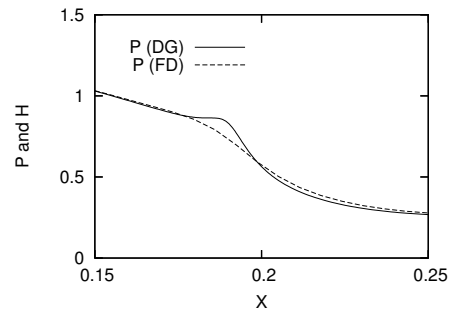
(a) $X_d = -0.9$



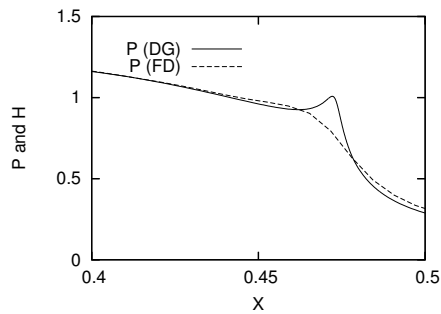
(b) $X_d = -0.6$



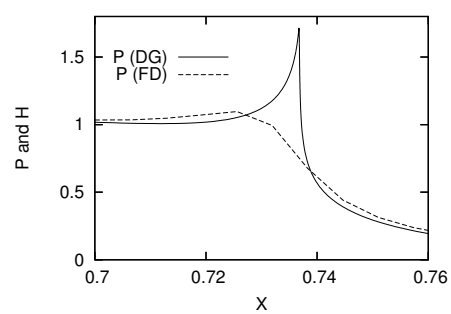
(c) $X_d = -0.3$



(d) $X_d = 0.3$



(e) $X_d = 0.6$



(f) $X_d = 0.9$

X_d	-2.0	-0.9	-0.6	-0.3	0.3	0.6	0.9
DG	-97.96	-166.3	-219.7	-126.7	-135.1	-136.6	-127.2
FD	-92.07	-161.5	-206.6	-108.0	-106.9	-118.1	-109.7